Materials Today Chemistry 35 (2024) 101854

Contents lists available at ScienceDirect

Materials Today Chemistry

journal homepage: www.journals.elsevier.com/materials-today-chemistry/

Synthesizing small-sized monodisperse molybdenum nanoparticles as potential precursors for medical radioisotopes

Á. Arnosa-Prieto *, M.A. González-Gómez, P. García-Acevedo, L. de Castro-Alves, Y. Piñeiro **, J. Rivas

NANOMAG Laboratory, Applied Physics Department, Materials Institute (iMATUS) and Health Research Institute of Santiago de Compostela (IDIS), Universidade de Santiago de Compostela, Santiago de Compostela, 15706, Spain

ARTICLE INFO

Keywords:
Molybdenum
Nanoparticles
Thermal decomposition
Hexacarbonylmolybdenum

ABSTRACT

Molybdenum-99 (^{99}Mo) is used to produce technetium-99 m (^{99m}Tc), one of the most used medical radioisotopes in the world. ^{99}Mo is currently created by fission of uranium-235 (^{235}U) in a small number of research nuclear fission reactors. Several problems related to the use of ^{235}U as primary source is causing a global ^{99}Mo generation crisis. Therefore, we are facing the need of finding new viable and safe production alternatives. Neutron activation of molybdenum is a promising candidate in which the ideal target for ^{99}Mo production are small monodisperse molybdenum nanoparticles (Mo NPs). However, the reported procedures for the obtention of Mo NPs present either the lack of simplicity of the employed synthetic methods or the inappropriate size and monodispersity of the synthesized Mo NPs. Here, we report a simple synthetic procedure for the obtention of small-sized monodisperse metallic Mo NPs. In the studied conditions, thermal decomposition of $Mo(CO)_6$ produced oleylamine coated Mo NPs. The oleylamine layer was included with the purpose of avoiding oxidation. Although an oxide patina was still formed on the surface of the Mo NPs, the core remains in a metallic phase after several weeks from its production, as it was confirmed by X-ray photoelectron spectroscopy analysis (XPS). The described synthetic procedure provides a simple method for the obtention of Mo NPs with optimum characteristics as non-fission method for ^{99}Mo production.

1. Introduction

Technetium-99 m (^{99m}Tc) isotope is a well-suited radionuclide for medical imaging thanks to its short half-life ($T_{1/2}$ = 6 h) and the low energy (140 keV) γ-ray emission. Radiopharmaceuticals based on ^{99m}Tc are the most used worldwide in Single Photon Emission Computed Tomography (SPECT) for the diagnosis of a variety of pathological conditions. ^{99m}Tc isotope is produced from the decay of molybdenum-99 (^{99}Mo), making ^{99}Mo an essential isotope in nuclear medicine [1,2].

^{99}Mo is currently produced from irradiation of uranium-235 (^{235}U) targets in a small number of research nuclear fission reactors in the world [3]. The Organization for Economic Co-operation and Development's Nuclear Energy Agency (OECD-NEA) has warned about a global ^{99}Mo supply crisis causing ^{99m}Tc shortages favored by different factors involved in materials obtained from ^{235}U [4]. The main problems are related to the production in nuclear research reactors that are approaching their lifespans because most of them were built within the same decade, the Non-Proliferation Treaty, and the subsequent generation and waste management issues associated with fission-produced ^{99}Mo [5,6]. Therefore, there is an urgent need to produce ^{99m}Tc radionuclide with new viable and safe methods to avoid the use of those based on ^{235}U fission [7].

Currently, the non-fission ^{99}Mo production relies on accelerator-based methods [8,9], with notable approaches being gamma-ray irradiation of ^{100}Mo and neutron activation of ^{98}Mo [1,10,11]. The neutron activation of ^{98}Mo method offers advantages such as generating less radioactive waste compared to the fission route, along with straightforward procedures and simple post-irradiation facilities [12,13]. In this method, natural or enriched molybdenum in the form of MoO_3 or bulk metallic molybdenum serves as the target for neutron bombardment. While both targets are viable, high purity metallic molybdenum is recommended, although it may result in low specific activity of ^{99}Mo with

* Corresponding author.
** Corresponding author.
E-mail addresses: angela.arnosa@usc.es (Á. Arnosa-Prieto), y.pineiro.redondo@usc.es (Y. Piñeiro).

https://doi.org/10.1016/j.mtchem.2023.101854
Received 6 August 2023; Received in revised form 5 December 2023; Accepted 8 December 2023
Available online 14 December 2023

some unreacted molybdenum [11,14].

It has been reported an approach that exploits the kinematic recoiling of the isotopes for their separation making the production process feasible. After irradiation, the recoiling nuclei will present sufficient kinetic energy to escape from the to the surrounding 'catcher' material, from which they will be further separated [15]. To be efficient, this method requires the use of small targets, such as thin foils or a suspension of nanoparticles.

In the case of the nanoparticles, an optimum size and monodispersity are required to avoid a decrease of the process efficiency. The nanoparticle size should be the smallest possible to allow the escape of the ^{99}Mo nuclei, and monodispersity is necessary to prevent the generation of unwanted nuclei from the NP surface sputtering. Polydisperse nanoparticles usually lead to the formation of agglomerates and hence an atom displaced by irradiation can escape from one single nanoparticle and interact with other nanoparticles from the same agglomerate, consequently causing undesired sputtered atoms [16]. Therefore, low small-sized monodisperse molybdenum nanoparticles are presented as the more appropriate target for the mentioned non-fission procedures.

Experimentally, monodisperse Mo NPs are difficult to produce either by chemical or physical synthesis [16] and some attempts are reported for their obtention either in suspension, or by supporting them on a substrate, from different synthetic procedures including electrical explosion of wires [17], physical vapor deposition (PVD) [18], laser ablation [19], thermal decomposition [20], sputtering methods [21,22], or the use of microorganisms [23]. Although thermal decomposition stands out for its simplicity to produce molybdenum nanoparticles in suspension, it still requires the use of particular equipment such as specific reactors [24]. Moreover, the produced materials, with average size values around 150 nm or between 30 nm and 50 nm in the smaller cases, exhibit a high polydispersity [24,25] and depart from the recommended small sizes to avoid unwanted nuclei generation in the sputtering surface [16].

In this groundbreaking study, we present a synthetic procedure for the production of small-sized metallic molybdenum nanoparticles (with a mean diameter around 10 nm) by harnessing the thermal decomposition of hexacarbonylmolybdenum [$Mo(CO)_6$] using readily available laboratory equipment. To ensure their stability and prevent oxidation, the nanoparticles are meticulously coated with a protective layer of oleylamine, ensuring reliable colloidal stability for subsequent physicochemical procedures. The simplicity and efficiency of this novel method differentiate it from previous approaches, underscoring its potential as a significant breakthrough in nanomaterial synthesis.

2. Materials and methods

2.1. Materials

Hexacarbonylmolybdenum ($MoCO_6$, 98 %) and trioctylamine ($C_{24}H_{51}N$, 70 %) were purchased from Acros Organics. Oleylamine ($C_{18}H_{37}N$, 70 %) was obtained from Aldrich. Ethanol (C_2H_6O, absolute) was purchased from Merck. Hexane (C_6H_{14}, 99 %) and acetone (C_2H_6O, pure) were obtained from Scharlau. All chemicals were used without any further purification.

2.2. Synthesis of oleylamine coated molybdenum nanoparticles (Mo@OLA NPs)

Oleylamine (4.5 mmol), $Mo(CO)_6$ (4.5 mmol) and 100 mL of trioctylamine were added to a 500 mL three-neck round bottomed flask. The temperature in the flask was raised to 330 °C and the mixture was mechanically stirred at 400 rpm under nitrogen atmosphere for 1 h. The solution turned black on the decomposition of hexacarbonylmolybdenum, indicating the formation of nanoparticles.

Once the reaction mixture was cooled down to room temperature, the product was washed with a mixture of deoxygenated solvents in proportions product:hexane:ethanol:acetone; 3.5:1.5:3:24 and centrifuged at 9000 rpm for 30 min. The supernatant was discarded, and the black precipitate was washed a second time with the previous solvent mixture in the same proportions and centrifugation conditions. The obtained solid was suspended in cyclohexane.

2.3. Characterization

The characterization of the crystalline phase of the nanoparticles was performed by powder X-ray diffraction (XRD) using a Philips diffractometer (Panalytical, Callo End, UK) with Cu Kα radiation (λ = 1.5406 Å). Measurements were collected in the 2θ angle range from 10° to 80° with steps of 0.04° and accounting time of 6 s per step. The morphology of the MNPs was characterized by transmission electron microscopy (TEM) using a JEOL JEM-1010 microscope (JEOL, Tokyo, Japan) operating at 100 kV and high-resolution transmission electron microscopy (HRTEM) using a JEOL JEM-2010-F microscope (JEOL, Tokyo, Japan) operating at 200 kV. Scanning electron microscopy (SEM) images were obtained using a Zeiss EVO LS15 microscope with energy dispersive X-ray spectroscopy (EDX) microanalysis (Zeiss, Oberkochen, Germany). X-ray photoelectron spectra (XPS) were acquired using a Thermofisher NEXSA spectrometer (Thermo Fisher Scientific, Madrid, Spain) equipped with a hemispherical electron analyzer and microfocused monochromatic aluminum Al Kα x-ray source (1486.6 eV). A monoatomic gun at 500 eV in series of 6 cycles of 30 s was used in the sputtering experiment. The Fourier transform infrared (FT-IR) spectra were recorded in a Thermo Nicolet Nexus spectrometer (Thermo Fisher Scientific, Madrid, Spain) using the attenuated total reflectance (ATR) method in the range 400–4000 cm^{-1}. Thermogravimetric analyses (TGA) were performed with sample previously dried at 50 °C for 3 h using a TGA PerkinElmer model 8000 (Perkin, Waltham, MA, USA) under a flowing nitrogen atmosphere of 20 mL min^{-1} at a temperature range from 50 °C to 850 °C at 10 °C per min.

3. Results and discussion

The powder X-ray diffractogram of Mo NPs, is presented in Fig. 1 together with the pattern for different species containing Mo, reveals the presence of pure molybdenum (COD card No. 9008474) [26], MoO_2 (COD card No. 1533435) [27] and MoO_3 (COD card No. 1537654) [28]. The position and relative intensity of the NPs diffraction peaks match the

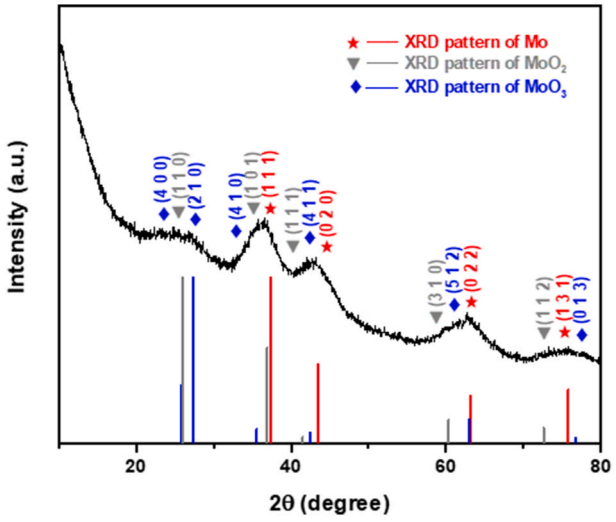

Fig. 1. Powder X-ray diffractogram of the prepared molybdenum nanoparticles (black) together with the pattern for molybdenum (red), MoO_2 (grey) and MoO_3 (blue). (For interpretation of the references to colour in this figure legend, the reader is referred to the Web version of this article.)

main theoretical Mo reflections, whose diffraction peaks at 36.9°, 43.0°, 62.8°, 75.7° respond to the (1 1 1), (0 2 0), (0 2 2) and (1 3 1) planes of cubic Mo lattice, respectively. The presence of broad peaks indicate also the contribution of some molybdenum oxides. The diffraction peak at 25.7° corresponds to the (1 1 0) plane of tetragonal MoO_2 lattice and to the (4 0 0) and (2 1 0) planes of orthorhombic MoO_3 lattice. The diffraction peaks at 36.9°, 43.0°, 62.8°, 75.7° present the contribution of the (1 0 1), (1 1 1), (3 1 0) and (1 1 2) planes of MoO_2 and the (4 1 0), (4 1 1), (5 1 2) and (0 1 3) planes of MoO_3, respectively. Moreover, the low relative intensity of these diffraction peaks indicate the existence of MoO_2 and MoO_3 in a smaller proportion related to the molybdenum (0) that can be due to the presence of an external layer of molybdenum oxides, which is further on identified by X-ray photoelectron spectroscopy (XPS).

Fig. 2 shows TEM and HRTEM images, size distribution and selected area electron diffraction (SAED) pattern of Mo NPs. From TEM image (Fig. 2a), it is observed that the NPs present nearly spherical morphology and with narrow size distribution. The average particle size of the NPs obtained from TEM images is 9.7 nm ± 2.4 nm and log-normal distribution is shown in Fig. 2b. SAED pattern presented in Fig. 2c shows a polycrystalline structure with defined ring, allowing the identification of the distances corresponding to the (1 1 1), (0 2 0), (0 2 2) and (1 3 1) planes of cubic Mo lattice. The magnified view of HRTEM image in Fig. 2d shows the good crystallinity of Mo nanoparticles. The lattice fringes (0.24 nm) that agree well with the spacing value of (1 1 1) lattice plane of Mo are clearly observed.

A SEM image of agglomerated Mo NPs in powder form is observed in Fig. 3a. To confirm and quantify the composition of the Mo nanoparticles, EDX line scans (Fig. 3b) were collected from the indicated area of the sample SEM image. An intense Mo signal with a percent by weight of 59.6 confirms that molybdenum is the main component of the nanoparticles. The existence of oxygen with a 17.1 wt% is in accordance with the presence of a molybdenum oxide surface layer of the nanoparticles. In addition, the lower percentage of O compared to Mo suggests that it present as a thin oxide layer, which is further confirmed by XPS. Nitrogen is not detected in the analysis, since the amount present in the sample is reduced to the nitrogen atoms of the oleylamine molecules constituting the coating layer, in a significantly smaller proportion compared to the metallic core of the nanoparticles. In consideration with this result, it is expected to obtain a small signal for carbon. Thus, the value of 23.1 wt% obtained for C may indicate some contribution to the signal from the adhesive carbon tab used to support the sample. The small aluminum signal with a 0.2 wt% can be assigned to adventitious aluminum, since it is not detected in the sample by any other used characterization technique and was not employed in the preparation of Mo NPs.

In addition, FT-IR spectrum of the obtained nanoparticles is shown in Fig. 4. Molybdenum oxides exhibit their main vibration modes in the 400–1000 cm^{-1} range. The bands observed at 685 cm^{-1}, 902 cm^{-1} and 950 cm^{-1} are characteristic of stretching mode of Mo═O and asymmetric and symmetric stretching modes of Mo–*O*–Mo, respectively [29, 30]. This bands indicate the presence of molybdenum oxides, which are located on the surface layer of the nanoparticles, as it is later demonstrated by XPS analysis.

Moreover, the presence of oleylamine as coating is confirmed by several bands involving C and N. The absorption band at 1600 cm^{-1} is associated to the C═C stretch mode [31] and the two bands at 2853 cm^{-1} and 2913 cm^{-1} correspond to the symmetric and asymmetric vibrations of the CH_2 group, respectively [32]. The band at 3055 cm^{-1} is assigned to the C–H stretching mode in C═C–H [33,34]. The broad shoulder centered at 3365 cm^{-1} is associated to the N–H stretching vibration [35].

Surface and core chemical state as well as the electronic structure of the Mo NPs was analysed by X-ray photoelectron spectroscopy (XPS). The XPS survey spectrum in Fig. 5a reveals the elemental composition of the sample's surface, where oxygen, nitrogen, carbon, and molybdenum,

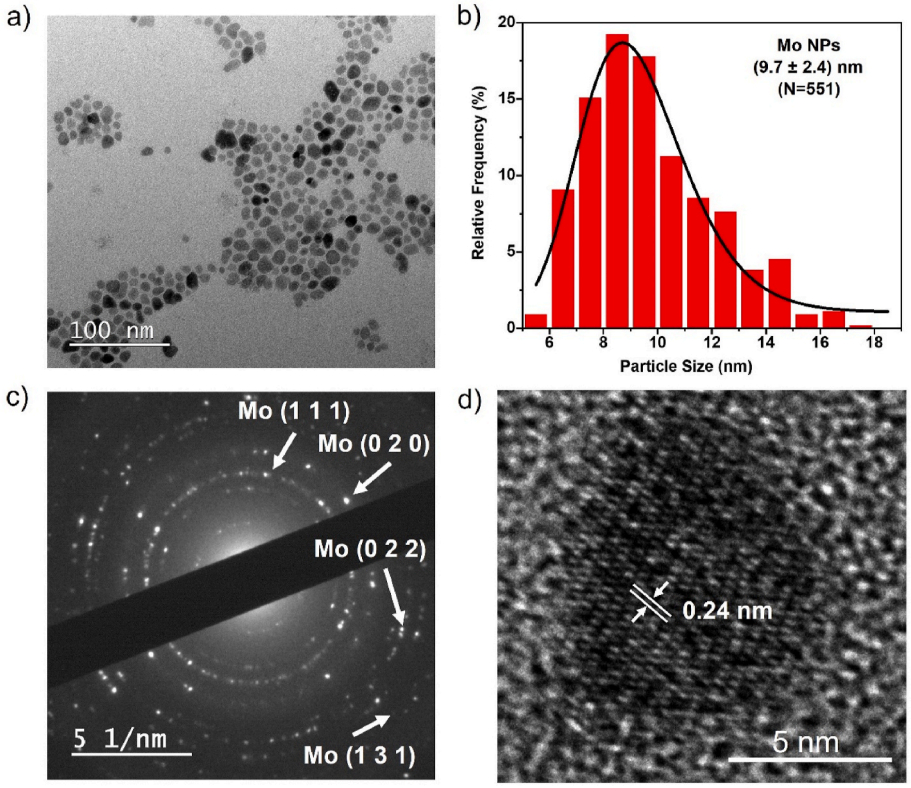

Fig. 2. TEM image (a) of the obtained molybdenum nanoparticles, size distribution (b) obtained by using the ImageJ software, selected area electron diffraction (SAED) pattern (c) and HRTEM image (d) of Mo NPs.

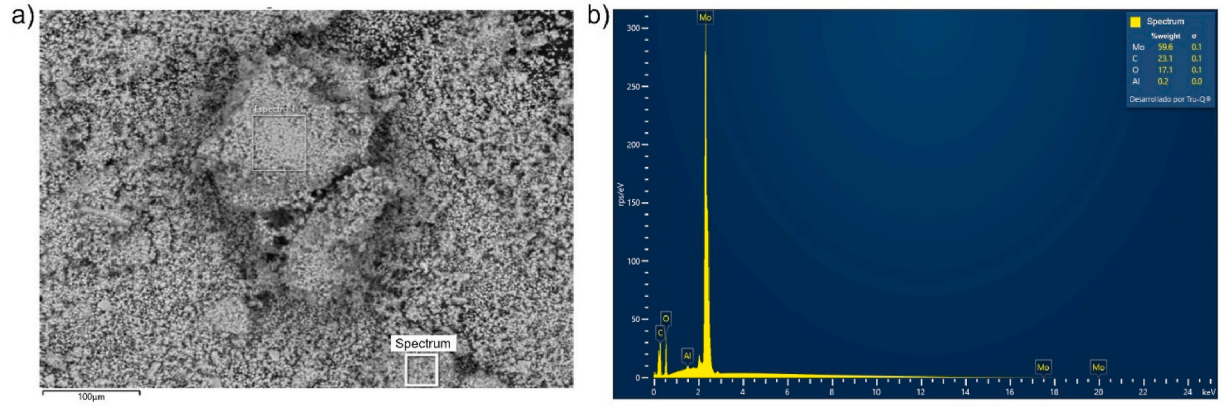

Fig. 3. SEM image showcasing powdered Mo NPs (a). EDX microanalysis providing quantification of elemental composition within the Mo NPs (b).

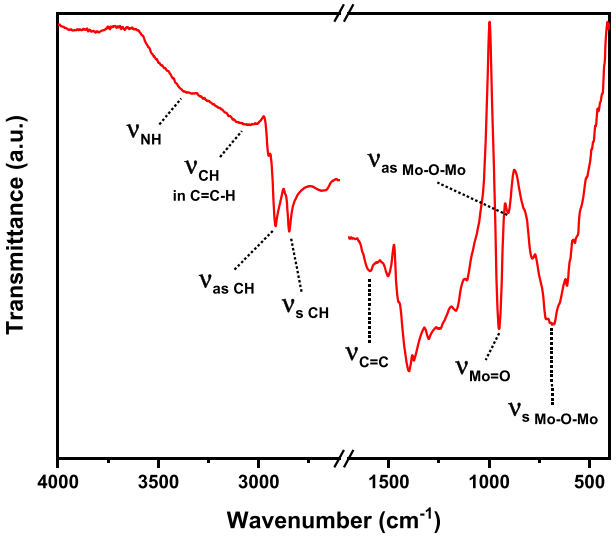

Fig. 4. FT-IR spectrum of the prepared oleylamine coated molybdenum nanoparticles with the identification of the main absorption bands.

can be identified at different binding energies. Quantification of the elemental composition using XPS survey spectra revealed atomic percentages of 52.08 % for carbon, 19.63 % for oxygen, 19.48 % for nitrogen and 8.81 % for molybdenum. The content of nitrogen and the large amount of carbon emerge from the oleylamine coating of the nanoparticles, while oxygen is consistent with the existence of a molybdenum oxide layer in the surface of the metallic core of the Mo NPs. Table 1S lists the values in wt% compared with the numbers acquired by EDX. XPS values differ from the quantification obtained by EDX since EDX provides bulk quantitative chemical analysis and XPS, surface quantitative chemical analysis. Thus, as oleylamine is present as a surface coating layer, the value obtained for carbon is higher when obtained by XPS and nitrogen is detected, while the values for molybdenum are considerably low due to the internal location in the Mo NPs. The binding energies and the atomic percents of the XPS spectra for Mo 3d, N 1s and C 1s are presented in Table 1. The data related to the peak fitting in Mo 3d, N 1s and C 1s spectra, including the peak area and full width at half maximum (FWMH), have been compiled in Table 2S, Tables 3S and 4S, respectively.

The deconvoluted XPS spectrum in Fig. 5b shows Mo 3d peaks, determining that the nanoparticles present an oxidized surface. None of the binding energies of Mo $3d_{3/2}$ and $3d_{5/2}$ correspond to Mo^0 since the energy at which usually assigns that state is lower than the registered, at around 228.0 eV [36]. The doublet peak structure at 232.53 eV and 235.60 eV is assigned to Mo^{6+} ion, as well as the peaks at 230.48 eV and 233.55 eV correspond to Mo^{4+} ion. For both Mo^{6+} and Mo^{4+}, these binding energies are in close agreement with reported values [37,38]. Peaks at binding energies of 229.19 eV and 232.32 eV correspond to an intermediate oxidation state, $Mo^{\delta+}$, $0 < \delta < 4$ [39]. The presence of molybdenum oxides (MoO_x) indicate the unavoidable surface oxidation of Mo^0 NPs even with the presence of a coating layer of oleylamine. The oxidation of the outer layers was expected since the nanoparticles are highly reactive.

The results of the deconvoluted peaks for N 1s are presented in Fig. 5c. The spectrum can be fit to three peaks with binding energies of 395.28 eV, 398.20 eV and 401.40 eV. The N 1s region is overlapped by a peak from molybdenum since the peak at 395.28 eV results from Mo $3p_{3/2}$ [40]. The most intense peak at 398.20 eV arises from the C–N bond between an aliphatic carbon and the nitrogen of the amine group [41]. The peak at 401.40 eV with a small atomic percentage associated (7.9 %) could be related to organic species involved in the preparation of Mo NPs (trioctylamine) trapped in the organic shell or absorbed on the nanoparticles [42]. The binding energy of the peak corresponds with the expected for the nitrogen of a tertiary amine [43], which is present in the trioctylamine.

Fig. 5d shows the deconvoluted peaks for C 1s for the synthesized nanoparticles. The peak at 283.27 eV is assigned to adventitious carbon [44,45]. The C 1s peak at 284.80 eV is ascribed to C–C/C═C bonds of oleylamine [46]. The peak at 286.15 eV corresponds to the C–N bond between a carbon and the nitrogen of the amine group [47]. The remaining peak at 288.65 eV presents an atomic percent contribution for carbon of 2.6 % that is within the 10 atomic percent experimental uncertainty. The experimental uncertainty associated with quantification is so large in comparison with the result that it can be considered no longer reliable or meaningful [48].

Sputtering experiments at low energy allow to assess the chemical state of an element at different depths inside a material by scanning the subsequent cycles underneath the material surface. The results of the sputtering experiment at a very low energy, 500 eV, in a series of six cycles of 30 s indicate the existence of an oxide patina on the surface of the metal, which practically disappears with the first cycle. The high resolution XPS spectrum of Mo 3d is shown in Fig. 6. After the first cycle, the peaks for a single chemical state can be observed, which are displaced to lower binding energies than the initial peaks. The peak corresponding to the Mo $3d_{5/2}$ appears after the first cycle at energies from 228.1 eV to 228.3 eV, corresponding to metallic Mo^0. The value for Mo^0 $3d_{5/2}$ binding energy is reported to be around 228.0 eV or 228.1 eV depending on the study [49,50]. The binding energy does not experience a change and, therefore, it is understood that metallic molybdenum is already reached. These findings suggest that the oxide layer is exceedingly thin, thus substantiating the remarkable achievement of reaching a predominantly metallic state.

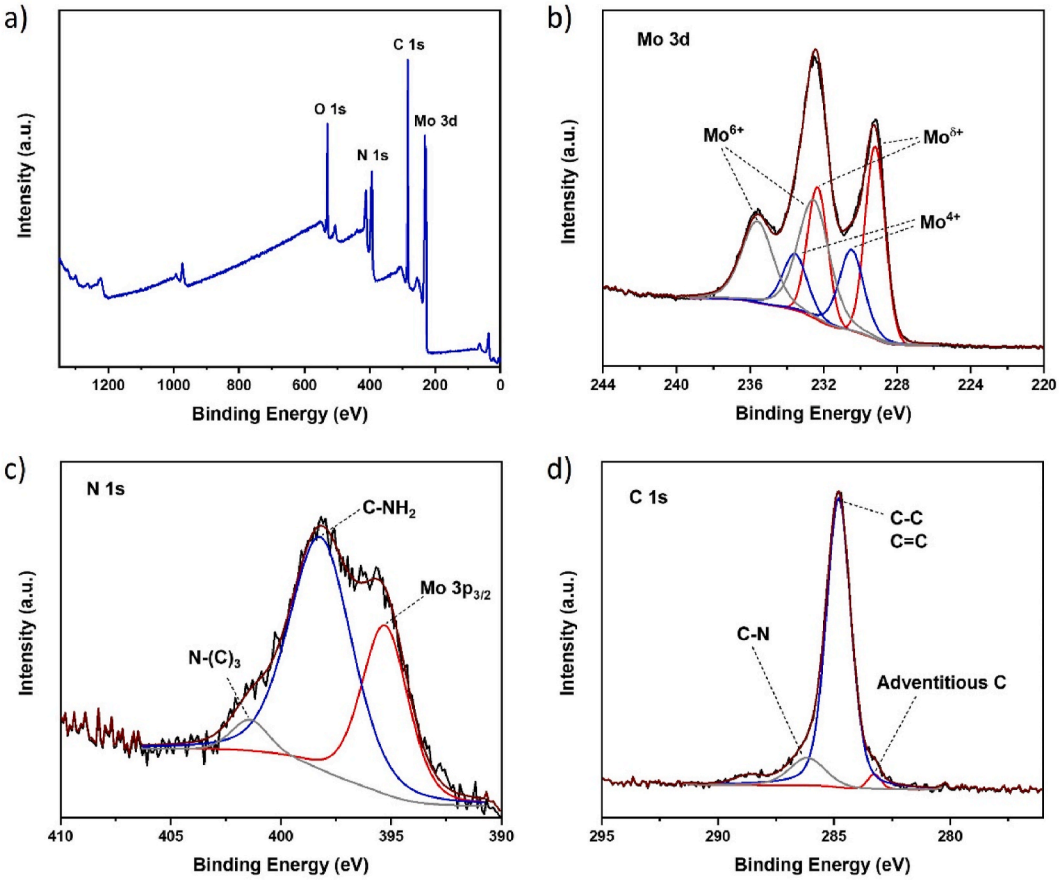

Fig. 5. XPS survey spectra (a) and deconvolution of the Mo 3d (b), N 1s (c) and C 1s (d) emission lines of Mo NPs.

Table 1
Binding energies and atomic percents for peaks in Mo 3d, N 1s and C 1s XPS spectra.

Element	Peak	Binding Energy [eV]	Atomic Percent (%)
Mo	$Mo^{\delta+}$, $0 < \delta < 4$	229.19/232.32	37.7
	Mo^{4+}	230.48/233.55	21.9
	Mo^{6+}	232.53/235.6	40.4
N	Mo $3p_{3/2}$	395.28	0
	C–NH_2	398.2	92.1
	N-$(C)_3$	401.4	7.9
C	Adventitious C	283.27	2.4
	C–C/C═C	284.80	83.6
	C–N	286.15	11.4

These data are also sustained by the results obtained from the O 1s XPS spectrum. Considering the high resolution XPS spectrum of O 1s shown in Fig. 7a, the peak corresponding to the patina of molybdenum oxides present at 532.0 eV practically disappears after the first cycle, and the remaining signal is linked to oleylamine. The behavior of the O 1s peak is in accordance with that observed for the Mo 3d peak, confirming that when the oxide patina is removed, Mo^0 appears. The high resolution XPS spectrum of C 1s in Fig. 7b corroborates that the signal of O 1s after the first cycle is attributed to the oleylamine, as the C 1s signal related to oleylamine is practically unchanged with the cycles. This also indicates that the oleylamine is very abundant in the nanoparticles.

TGA and derivative curves of Mo NPs are presented in Fig. 8. The mass loss around 1 % between 50 °C and 110 °C is consistent with the desorption of physisorbed water in the powder sample. A significant mass loss around 19 % is detected from 120 °C to 500 °C corresponding to the degradation of the oleylamine coating layer of the nanoparticles [51]. Between 630 °C and 820 °C, with a strong peak centered at 790 °C

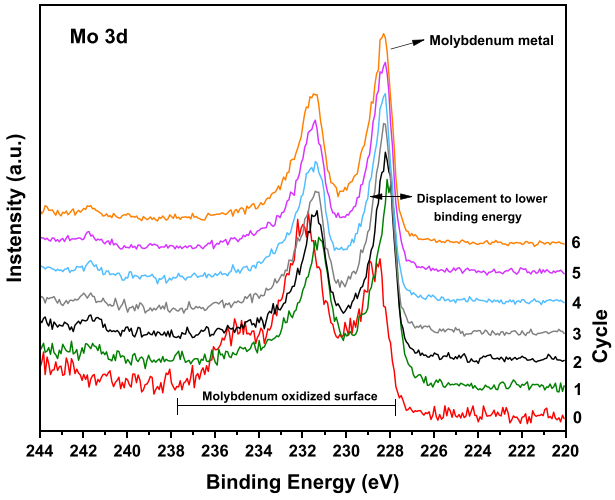

Fig. 6. High resolution Mo 3d XPS spectra when applying six sputtering cycles.

in the derivative curve, a mass loss of nearly 18 % is produced by the volatilization of MoO_3 and, might also include other MO_x. The degree of volatilization of MoO_3 is noticeable as the temperature increases above 750 °C, specially at 780 °C or more [52], which is in agreement with the results.

The thermal decomposition method described in this study yields molybdenum nanoparticles that surpass previous reported procedures in terms of both small-size characteristics and monodispersity. The advancements present an improvement in the synthesis of suspended Mo NPs. Zamora-Romero and coworkers reported a procedure to obtain Mo

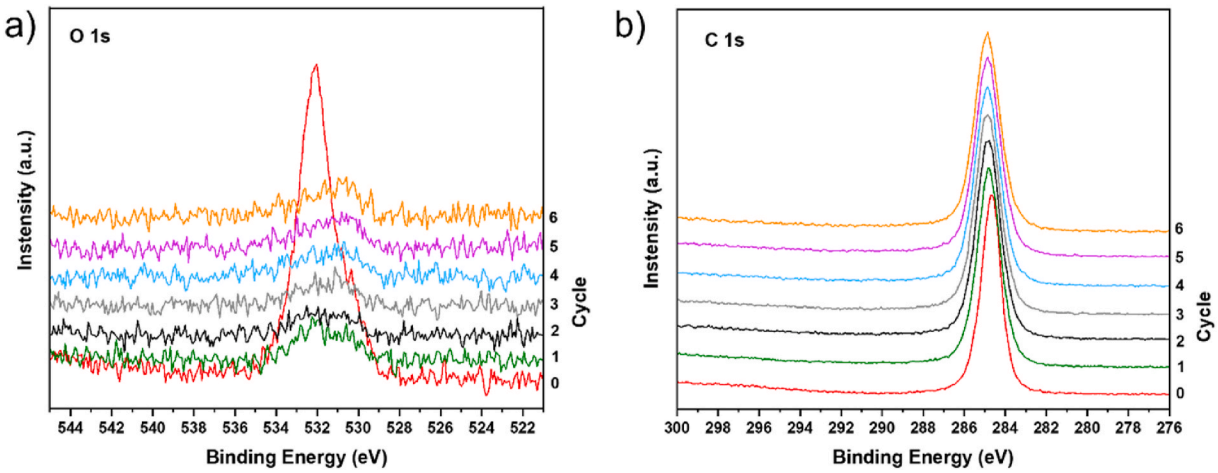

Fig. 7. High resolution O 1s XPS spectra (a) and C 1s XPS spectra (b) when applying six sputtering cycles.

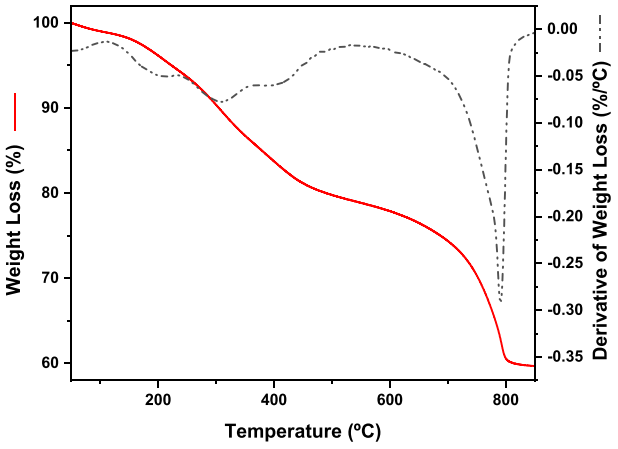

Fig. 8. TGA and derivative curves of oleylamine coated molybdenum nanoparticles.

NPs in suspension through laser ablation. Their results showed quasi-spherical agglomerates with broad Mo NPs size distributions. Their smallest Mo NPs presented a TEM average particle size of 48 nm, however the size distribution included NPs up to 180 nm [19]. Nordmeier and coworkers presented Mo NPs synthesized by microorganisms, with a size distribution of the nanoparticles ranged from 9 to 95 nm obtained from TEM analysis and a nearly spherical morphology [23]. Other authors selected thermal decomposition as synthetic method for producing Mo NPs. Redel and coworkers incorporated ionic liquids to the thermal decomposition of $Mo(CO)_6$. The reported Mo NPs presented an average particle size of 150 nm and the authors clearly stated the lack of monodispersity [25]. The design of a specific reaction chamber for thermal decomposition was reported by Huh and coworkers. The produced Mo NPs were nearly square in shape and two different populations of particle size coexisted in the final product. Small particles with a size distribution between 2.0 nm and 3.0 nm and large particles with a wide size distribution between 30.0 nm and 50.0 nm were found together in suspension [24]. Thus, the overall view of the reported methods for the obtention of Mo NPs in solution evidences the lack of monodispersity and small size in the products. In comparison to these findings, the synthetic procedure presented in this study achieves a remarkable reduction in Mo NPs size to 9.7 nm ± 2.4 nm, with a narrow size distribution, and stands out by its simplicity and efficiency, using only conventional laboratory glassware and equipment along with common laboratory solvents.

4. Conclusions

In this work, molybdenum nanoparticles were synthesized through thermal decomposition of $Mo(CO)_6$. To prevent oxidation, a protective coating layer of oleylamine was included. The resulting Mo NPs exhibited smaller size (9.7 nm ± 2.4 nm) and higher monodispersity compared to previously reported methods using thermal decomposition. The presence of the oleylamine layer was confirmed through FTIR analysis and its preservation was evident from the observed decomposition in the TGA curve. X-ray diffraction analysis indicated the presence of both metallic molybdenum and molybdenum oxide in the Mo NPs. This was further supported by XPS analysis, which revealed a metallic molybdenum core surrounded by a MoO_x layer forming the Mo NPs. The formation of an oxide patina on the Mo NPs' surface, resulting from the inherent reactivity of Mo^0 NPs, was expected despite the oleylamine coating. The developed synthetic procedure for obtaining small-sized and monodisperse Mo NPs holds potential as a suitable molybdenum source for the exploration of non-fission techniques in ^{99}Mo production studies.

CRediT authorship contribution statement

Á. Arnosa-Prieto: Conceptualization, Investigation, Methodology, Writing - original draft, Writing - review & editing. **M.A. González-Gómez:** Investigation, Methodology. **P. García-Acevedo:** Methodology, Writing - review & editing. **L. de Castro-Alves:** Writing - review & editing. **Y. Piñeiro:** Conceptualization, Supervision, Writing - review & editing. **J. Rivas:** Funding acquisition, Supervision, Writing - review & editing.

Declaration of competing interest

The authors declare that they have no known competing financial interests or personal relationships that could have appeared to influence the work reported in this paper.

Data availability

Data will be made available on request.

Acknowledgements

We thank Prof. Carlos Vázquez Vázquez for his invaluable advice. This work was supported by the Programa de Axudas de apoio á etapa predoutoral 2020 of Xunta de Galicia, by the European Commission under the BOW project (FETPROACT-EIC-05-2019, Grant 952183),

CARTsol project (PLEC2022-009217 funded by MICINN/AEI/10.13039/501100011033 and NextGenerationEU/PRTR) and partially supported by the Spanish Ministry of Science and Innovation (ref PID2020-112626RB-C21), Modalities « Research Challenges» and «Knowledge Generation» and the Regional Consellería de Innovación Program for the Grupos de Referencia Competitiva 2021 —GRC2021 project of Xunta de Galicia.

Appendix A. Supplementary data

Supplementary data to this article can be found online at https://doi.org/10.1016/j.mtchem.2023.101854.

References

[1] M. Capogni, A. Pietropaolo, L. Quintieri, M. Angelone, A. Boschi, M. Capone, N. Cherubini, P. De Felice, A. Dodaro, A. Duatti, A. Fazio, S. Loreti, P. Martini, G. Pagano, M. Pasquali, M. Pillon, L. Uccelli, A. Pizzuto, 14 MeV neutrons for99Mo/99mTc production: experiments, simulations and perspectives, Molecules 23 (2018) 1872–1892, https://doi.org/10.3390/molecules23081872.

[2] IAEA, Feasibility of Producing Molybdenum-99 on a Small Scale Using Fission of Low Enriched Uranium or Neutron Activation of Natural Molybdenum, 2015. http://www-pub.iaea.org/books/IAEABooks/10599/Feasibility-of-Producing-Molybdenum-99-on-a-Small-Scale-Using-Fission-of-Low-Enriched-Uranium-or-Neutron-Activation-of-Natural-Molybdenum.

[3] M. Gumiela, Cyclotron production of 99mTc: comparison of known separation technologies for isolation of 99mTc from molybdenum targets, Nucl. Med. Biol. 58 (2018) 33–41, https://doi.org/10.1016/j.nucmedbio.2017.11.001.

[4] M. Wenzl, F. Colombo, F. Guanais, R. Lopert, V. Paris, M. Pearson, K. Charlton, S. J. Demeter, S. Bilbao y Leon, C. Pike, O. Kvarnstroem, C.A. Hernandez, A. Perkins, The Supply of Medical Isotopes: an Economic Diagnosis and Possible Solutions, Organisation for Economic Co-Operation and Development, 2019, https://doi.org/10.1787/9b326195-en.

[5] M.R.A. Pillai, A. Dash, F.F. Russ Knapp, Diversification of 99Mo/99mTc separation: non-fission reactor production of 99Mo as a strategy for enhancing 99mTc availability, J. Nucl. Med. 56 (2015) 159–161, https://doi.org/10.2967/jnumed.114.149609.

[6] M.R.A. Pillai, A. Dash, F.F. Knapp, Sustained availability of 99mTc: possible paths forward, J. Nucl. Med. 54 (2013) 313–323, https://doi.org/10.2967/jnumed.112.110338.

[7] G.M. Contessa, M. D'Arienzo, M. Frisoni, P. Ferrari, R. Panichi, F. Moro, A. Pietropaolo, Preliminary evaluations of the environmental impact for the production of 99Mo by fusion neutrons, Eur. Phys. J. Plus. 136 (2021), https://doi.org/10.1140/epjp/s13360-021-01404-0.

[8] M.F. Nawar, A. Türler, New strategies for a sustainable 99mTc supply to meet increasing medical demands: promising solutions for current problems, Front. Chem. 10 (2022), https://doi.org/10.3389/fchem.2022.926258.

[9] M. Inagaki, S. Sekimoto, T. Tadokoro, Y. Ueno, Y. Kani, T. Ohtsuki, Production of 99Mo/99mTc by photonuclear reaction using a natMoO3 target, J. Radioanal. Nucl. Chem. 324 (2020) 681–686, https://doi.org/10.1007/s10967-020-07086-9.

[10] M. Lin, W. Tian, J. Wang, R. Gao, F. Fan, Z. Qin, S. Cao, Z. Ran, Optimization of target system for the production of 99Mo via 100Mo(γ,n)99Mo reaction, Appl. Radiat. Isot. 202 (2023), 111059, https://doi.org/10.1016/j.apradiso.2023.111059.

[11] S. Hasan, M.A. Prelas, Molybdenum-99 production pathways and the sorbents for 99Mo/99mTc generator systems using (n, γ) 99Mo: a review, SN Appl. Sci. 2 (2020) 1–28, https://doi.org/10.1007/s42452-020-03524-1.

[12] N.P. Dikiy, A.N. Dovbnya, N.V. Krasnoselsky, Y.V. Lyashko, E.P. Medvedeva, D. V. Medvedev, V.L. Uvarov, I.D. Fedorets, The use of molybdenum oxide nanoparticles for production of free isotope Mo-99, Probl. At. Sci. Technol. 100 (2015) 154–156.

[13] M. Munir, Sriyono Herlina, E. Sarmini, Abidin, H. Lubis, Marlina, influence of GA siwabessy reactor irradiation period on the molybdenum-99 (99Mo) production by neutron activation of natural molybdenum to produce technetium-99m (99mTc), J. Phys. Conf. Ser. 1204 (2019), https://doi.org/10.1088/1742-6596/1204/1/012021.

[14] I. Cieszykowska, K. Jerzyk, M. Żółtowska, T. Janiak, G. Birnbaum, Studies on electrochemical dissolution of sintered molybdenum discs as a potential method for targets dissolution in 99mTc production, J. Radioanal. Nucl. Chem. 331 (2022) 1029–1037, https://doi.org/10.1007/s10967-021-08155-3.

[15] V.N. Starovoitova, L. Tchelidze, D.P. Wells, Production of medical radioisotopes with linear accelerators, Appl. Radiat. Isot. 85 (2014) 39–44, https://doi.org/10.1016/j.apradiso.2013.11.122.

[16] C. Panetier, A. Ruiz-Moreno, F. Rossi, T. Roubille, G. Zerovnik, A. Plompen, N. Moncoffre, Y. Pipon, Molecular dynamics simulations of Mo nanoparticles sputtering under irradiation, Phys. Scripta 97 (2022), 125003, https://doi.org/10.1088/1402-4896/ac9c9f.

[17] Y.S. Kwon, A.P. Ilyin, O.B. Nazarenko, D.V. Tikhonov, G.V. Yablunovsky, Fabrication of molybdenum nanopowders by electrical explosion of wires, Proc. IFOST-2008 - 3rd Int. Forum Strateg. Technol. (2008) 217–219, https://doi.org/10.1109/IFOST.2008.4602897.

[18] D.V. Potapenko, J.M. Horn, R.J. Beuhler, Z. Song, M.G. White, Reactivity studies with gold-supported molybdenum nanoparticles, Surf. Sci. 574 (2005) 244–258, https://doi.org/10.1016/j.susc.2004.10.035.

[19] N. Zamora-Romero, M.A. Camacho-Lopez, M. Camacho-Lopez, A.R. Vilchis-Nestor, V.H. Castrejon-Sanchez, S. Camacho-Lopez, G. Aguilar, Molybdenum nanoparticles generation by pulsed laser ablation and effects of oxidation due to aging, J. Alloys Compd. 788 (2019) 666–671, https://doi.org/10.1016/j.jallcom.2019.02.270.

[20] S. Jaenicke, W.L. Loh, Preparation of highly dispersed molybdenum on alumina by thermal decomposition of Mo(CO)6, Catal. Today 49 (1999) 123–130, https://doi.org/10.1016/S0920-5861(98)00416-7.

[21] A.S. Edelstein, G.M. Chow, E.I. Altman, R.J. Colton, D.M. Hwang, Self-arrangement of molybdenum particles into cubes, 80-, Science 251 (1991) 1590–1592, https://doi.org/10.1126/science.251.5001.1590.

[22] A.S. Edelstein, Formation threshold and structural evolution of molybdenum nanocrystals with sputtering pressure, J. Mater. Res. 6 (1991) 8–10, https://doi.org/10.1557/JMR.1991.0008.

[23] A. Nordmeier, A. Merwin, D.F. Roeper, D. Chidambaram, Microbial synthesis of metallic molybdenum nanoparticles, Chemosphere 203 (2018) 521–525, https://doi.org/10.1016/j.chemosphere.2018.02.079.

[24] S.H. Huh, S.J. Oh, Y.N. Kim, G.H. Lee, A design of a nanometer size metal particle generator: thermal decomposition of metal carbonyls, Rev. Sci. Instrum. 70 (1999) 4366–4369, https://doi.org/10.1063/1.1150081.

[25] E. Redel, R. Thomann, C. Janiak, Use of ionic liquids (ILs) for the IL-anion size-dependent formation of Cr, Mo and W nanoparticles from metal carbonyl M(CO)6 precursors, Chem. Commun. (2008) 1789–1791, https://doi.org/10.1039/b718055a.

[26] R.W.G. Wyckoff, Crystal structures, Am. Mineral. Cryst. Struct. Database. 1 (1963) 7–83.

[27] G.A. Seisenbaeva, M. Sundberg, M. Nygren, L. Dubrovinsky, V.G. Kessler, Thermal decomposition of the methoxide complexes MoO(OMe)4, Re4O6(OMe)12 and (Re1-xMox)O6(OMe)12 ($0.24 \leq x \leq 0.55$), Mater. Chem. Phys. 87 (2004) 142–148, https://doi.org/10.1016/j.matchemphys.2004.05.025.

[28] G. Andersson, A. Magnéli, On the crystal structure of molybdenum trioxide, Acta Chem. Scand. 4 (1950) 793–797, https://doi.org/10.3891/acta.chem.scand.04-0793.

[29] C.V. Subba Reddy, Y.Y. Qi, W. Jin, Q.Y. Zhu, Z.R. Deng, W. Chen, S. Il Mho, An electrochemical investigation on (MoO3+PVP+PVA) nanobelts for lithium batteries, J. Solid State Electrochem. 11 (2007) 1239–1243, https://doi.org/10.1007/s10008-007-0278-4.

[30] I. Kostis, N. Vourdas, G. Papadimitropoulos, A. Douvas, M. Vasilopoulou, N. Boukos, D. Davazoglou, Effect of the oxygen sub-stoichiometry and of hydrogen insertion on the formation of intermediate bands within the gap of disordered molybdenum oxide films, J. Phys. Chem. C 117 (2013) 18013–18020, https://doi.org/10.1021/jp407354j.

[31] X. Lu, H.Y. Tuan, B.A. Korgel, Y. Xia, Facile synthesis of gold nanoparticles with narrow size distribution by using AuCl or AuBr as the precursor, Chem. Eur J. 14 (2008) 1584–1591, https://doi.org/10.1002/chem.200701570.

[32] M. Chen, Y.G. Feng, X. Wang, T.C. Li, J.Y. Zhang, D.J. Qian, Silver nanoparticles capped by oleylamine: formation, growth, and self-organization, Langmuir 23 (2007) 5296–5304, https://doi.org/10.1021/la700553d.

[33] S. Mourdikoudis, M. Menelaou, N. Fiuza-Maneiro, G. Zheng, S. Wei, J. Pérez-Juste, L. Polavarapu, Z. Sofer, Oleic acid/oleylamine ligand pair: a versatile combination in the synthesis of colloidal nanoparticles, Nanoscale Horizons 7 (2022) 941–1015, https://doi.org/10.1039/d2nh00111j.

[34] S. Mourdikoudis, L.M. Liz-Marzán, Oleylamine in nanoparticle synthesis, Chem. Mater. 25 (2013) 1465–1476, https://doi.org/10.1021/cm4000476.

[35] T. Togashi, M. Nakayama, A. Hashimoto, M. Ishizaki, K. Kanaizuka, M. Kurihara, Solvent-free synthesis of monodisperse Cu nanoparticles by thermal decomposition of an oleylamine-coordinated Cu oxalate complex, Dalton Trans. 47 (2018) 5342–5347, https://doi.org/10.1039/c8dt00345a.

[36] I. Takano, S. Isobe, T.A. Sasaki, Y. Baba, Nitrogenation of various transition metals by N+2-ion implantation, Appl. Surf. Sci. 37 (1989) 25–32, https://doi.org/10.1016/0169-4332(89)90970-7.

[37] D.O. Scanlon, G.W. Watson, D.J. Payne, G.R. Atkinson, R.G. Egdell, D.S.L. Law, Theoretical and experimental study of the electronic structures of MoO3 and MoO2, J. Phys. Chem. C 114 (2010) 4636–4645, https://doi.org/10.1021/jp9093172.

[38] J. Baltrusaitis, B. Mendoza-Sanchez, V. Fernandez, R. Veenstra, N. Dukstiene, A. Roberts, N. Fairley, Generalized molybdenum oxide surface chemical state XPS determination via informed amorphous sample model, Appl. Surf. Sci. 326 (2015) 151–161, https://doi.org/10.1016/j.apsusc.2014.11.077.

[39] G.T. Kim, T.K. Park, H. Chung, Y.T. Kim, M.H. Kwon, J.G. Choi, Growth and characterization of chloronitroaniline crystals for optical parametric oscillators. I. XPS study of Mo-based compounds, Appl. Surf. Sci. 152 (1999) 35–43, https://doi.org/10.1016/S0169-4332(99)00293-7.

[40] X. Lang, M.A. Qadeer, G. Shen, R. Zhang, S. Yang, J. An, L. Pan, J.J. Zou, A Co-Mo2N composite on a nitrogen-doped carbon matrix with hydrogen evolution activity comparable to that of Pt/C in alkaline media, J. Mater. Chem. A 7 (2019) 20579–20583, https://doi.org/10.1039/c9ta07749a.

[41] S. Marzorati, E.M. Ragg, M. Longhi, L. Formaro, Low-temperature intermediates to oxygen reduction reaction catalysts based on amine-modified metal-loaded carbons. An XPS and ss-NMR investigation, Mater. Chem. Phys. 162 (2015) 234–243, https://doi.org/10.1016/j.matchemphys.2015.05.063.

[42] A. Zakhtser, A. Naitabdi, R. Benbalagh, F. Rochet, C. Salzemann, C. Petit, S. Giorgio, Chemical evolution of Pt-Zn nanoalloys dressed in oleylamine, ACS Nano 15 (2021) 4018–4033, https://doi.org/10.1021/acsnano.0c03366.

[43] S. Ravi, S. Zhang, Y.R. Lee, K.K. Kang, J.M. Kim, J.W. Ahn, W.S. Ahn, EDTA-functionalized KCC-1 and KIT-6 mesoporous silicas for Nd3+ ion recovery from aqueous solutions, J. Ind. Eng. Chem. 67 (2018) 210–218, https://doi.org/10.1016/j.jiec.2018.06.031.

[44] A.E. Coumans, E.J.M. Hensen, A model compound (methyl oleate, oleic acid, triolein) study of triglycerides hydrodeoxygenation over alumina-supported NiMo sulfide, Appl. Catal. B Environ. 201 (2017) 290–301, https://doi.org/10.1016/j.apcatb.2016.08.036.

[45] N. Nordin, W.Z. Samad, M.R. Yusup, M.R. Othman, Synthesis and characterization of copper(II) carboxylate with palm-based oleic acid by, Malaysian J. Anal. Sci. 19 (2015) 236–243.

[46] D. Wilson, M.A. Langell, XPS analysis of oleylamine/oleic acid capped Fe3O4 nanoparticles as a function of temperature, Appl. Surf. Sci. 303 (2014) 6–13, https://doi.org/10.1016/j.apsusc.2014.02.006.

[47] Y. Hou, Z.R. Zhou, T.Y. Wen, H.W. Qiao, Z.Q. Lin, B. Ge, H.G. Yang, Enhanced moisture stability of metal halide perovskite solar cells based on sulfur-oleylamine surface modification, Nanoscale Horizons 4 (2019) 208–213, https://doi.org/10.1039/c8nh00163d.

[48] T.R. Gengenbach, G.H. Major, M.R. Linford, C.D. Easton, Practical guides for x-ray photoelectron spectroscopy (XPS): interpreting the carbon 1s spectrum, J. Vac. Sci. Technol. A 39 (2021), 013204, https://doi.org/10.1116/6.0000682.

[49] K.S. Kim, W.E. Baitinger, J.W. Amy, N. Winograd, ESCA studies of metal-oxygen surfaces using argon and oxygen ion-bombardment, J. Electron. Spectrosc. Relat. Phenom. 5 (1974) 351–367, https://doi.org/10.1016/0368-2048(74)85023-1.

[50] S.L.T. Andersson, R.F. Howe, An X-ray photoelectron study of metal clusters in zeolites, J. Phys. Chem. 93 (1989) 4913–4920, https://doi.org/10.1021/j100349a047.

[51] M. Menelaou, K. Georgoula, K. Simeonidis, C. Dendrinou-Samara, Evaluation of nickel ferrite nanoparticles coated with oleylamine by NMR relaxation measurements and magnetic hyperthermia, Dalton Trans. 43 (2014) 3626–3636, https://doi.org/10.1039/c3dt52860j.

[52] A.L. Al-Alotaibi, N. Altamimi, E. Howsawi, K.A. Elsayed, I. Massoudi, A. E. Ramadan, Synthesis and characterization of MoO3 for photocatalytic applications, J. Inorg. Organomet. Polym. Mater. 31 (2021) 2017–2029, https://doi.org/10.1007/s10904-021-01939-w.